2D MXenes: Tunable Mechanical and Tribological Properties

Brian C. Wyatt, Andreas Rosenkranz, and Babak Anasori

2D transition metal carbides, nitrides, and carbonitrides, known as MXenes, were discovered in 2011 and have grown to prominence in energy storage, catalysis, electromagnetic interference shielding, wireless communications, electronic, sensors, environmental and biomedical applications. In addition to their high electrical conductivity and electrochemically active behavior, MXenes' mechanical properties, flexibility, and strong adhesion properties play a crucial role in almost all of these growing applications. Although these properties prove to be critical in MXenes' impressive performance, the mechanical and tribological understanding of MXenes, as well as their relation to the synthesis process, is yet to be fully explored. In this perspective, a fundamental overview of MXenes' mechanical and tribological properties is provided and the effects of MXenes' compositions, synthesis, and processing steps on these properties are discussed. Additionally, we provide a critical perspective of the compositional control of MXenes for innovative structural, low-friction, and low-wear performance in current and upcoming applications of MXenes. This perspective establishes that the fundamental understanding of MXenes' mechanical and tribological behavior is essential for their quickly growing applications.

1. Introduction

With the exponential expansion of two-dimensional (2D) materials since 2004, these nanomaterials have gained notable attention in many applications including energy storage,[1] catalysis,[8] flexible electronics,[9] and triboelectric nanogenerators.[12] MXenes, discovered in 2011, are a few-atom thick layered 2D transition metal carbides, nitrides, and carbonitrides.[13] MXene single flakes are denoted with the chemical formula $M_{n+1}X_nT_x$ (n = 1 to 4), which describes alternating layers of transition metals (M: groups 3 – 6 of the periodic table) interleaved with layers of carbon/nitrogen (X) with bonded terminations (T_x: -O_2, -F_2, -$(OH)_2$, -Cl_2 or their combinations) on the exterior transition metal surface.[6, 14, 15] MXenes' crystal structures and chemical formula are derived from their 3D crystalline precursors, which are usually MAX phases.[18] MAX phases are chemically denoted by $M_{n+1}AX_n$ (n = 1 to 4), for which the M-X layers found in MXenes are sandwiched by layers of A-group elements (mostly group 13-16 of the periodic table).[21] MXenes are synthesized by selectively removing/etching these A-group element layers. Upon the removal of these A layers, surface terminations (T_x) occupy the bonding sites on M layers previously bonded to the A-group elements.[28]

MXenes are excellent candidates for a range of applications (Figure 1a), including energy storage, [6] transparent electronics,[30, 31] sensors,[32] electromagnetic interference (EMI) shielding,[33, 34] and catalysis.[35] These applications involve MXenes as flexible and thin films,[31] MXenes as anchors in hybrid materials,[36] embedded in matrix materials,[25, 37] or even as wearable fabrics.[38] In almost all these applications, fundamental understanding of the mechanical and tribological properties of MXenes is necessary (Figure 1b). The mechanical properties are vital to MXenes' applications in energy storage and catalysis, as MXenes in electrodes can act as active materials, conductive additives, strong binders, and current collectors, which can control the structure of the electrode and withstand expansion and contraction during charge and discharge cycles.[6, 39] Additionally, the rise of flexible and wearable devices [31, 38, 40] necessitates mechanical characterization of MXene to withstand the required mechanical forces while maintaining the flexibility for these applications. Similarly, the potential applications of MXenes in triboelectric nanogenerators for energy storage and wearable electronics requires the characterization of MXenes' tribological properties.[41] More recently, MXenes have been used as reinforcement phases in composite materials.[42] The relevance of the mechanical and tribological properties in various applications is illustrated in Figure 1b. The rationale and support for this figure is summarized in Figures S1and S2 and discussed further in the Supporting Information.

Despite well over 3000 publications to date on MXenes since their discovery,[43] only 4.9% of

B. C. Wyatt, Prof. B. Anasori
Department of Mechanical and Engineering, and Integrated Nanosystems Development Institute
Purdue School of Engineering and Technology
Indiana University-Purdue University
Indianapolis, IN 46202, USA
E-mail: banasori@iupui.edu

Prof. A. Rosenkranz
Department of Chemical Engineering
Biotechnology and Materials
FCFM
Universidad de Chile
Santiago, Chile
E-mail: arosenkranz@ing.uchile.cl

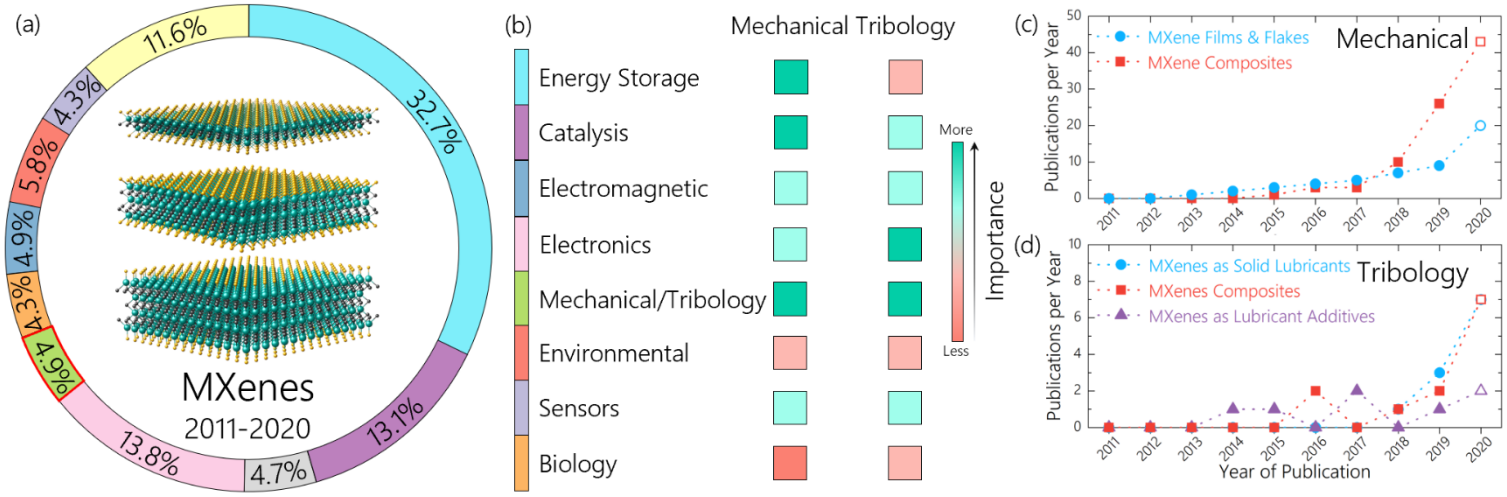

Figure 1. Main applications of MXenes and the importance of the mechanical and tribological properties to those applications. (a) Through a systematic analysis of all current publications on MXenes (up to August 2020), only 4.9% of publications focus on either the mechanical or tribological properties of MXenes. (b) The scale of the importance of the mechanical or tribological properties of MXenes in each application category. Detailed analysis of the importance of both mechanical and tribology properties to each application is described in the Supporting Information. (c) The total number of publications to date on mechanical characterization of MXenes in film or single flake forms as well as MXenes in different matrices (MXene composites). Predicted publications in 2020 based on publications up to August of 2020 are shown in non-shaded markers. (d) The total tribological publications to date, where the categories are defined by solid lubricants, lubricant additives, and composites. Solid lubricants consider the use of MXene layers on the surface of a substrate material under dry conditions, while lubricant additives involve MXenes dispersed in oil or water. Composites denotes the use of MXenes in different matrices to improve the resulting friction and wear performance. Predicted publications in 2020 based on publications up to August of 2020 are shown in non-shaded markers.

publications have studied their mechanical and tribological properties and their applications as reinforcement materials in composites, as shown in Figure 1a. Only two experimental studies on the mechanical stiffness and strength of MXene single flakes have been published on $Ti_3C_2T_x$ [16] and $Nb_4C_3T_x$.[19] In addition, only one experimental study on the adhesion properties exist on Ti_2CT_x and $Ti_3C_2T_x$ MXenes in suspended layers of single flakes.[44] The total number of publications per year on the mechanical and tribological properties of MXenes and their composites are highlighted in Figures 1c and d, respectively, which show the rapid growth of this field. Additionally, MXenes are a highly expansive family of nanomaterials, as there are well over 70 possible compositions of mono-transition metal MXenes and limitless double-transition metal MXenes in form of ordered and solid solutions.[45] MXenes' inherent ability to tune properties through use of different transition metal(s), carbon/nitrogen, and surface functionalities is unique to the field of 2D nanomaterials. The significant potential of the atomistic design of MXenes in mechanical and tribological applications requires fundamental understanding of the effects induced by MXenes' composition and synthesis route.

In this perspective, we first survey the effect of the synthesis route on MXenes' structure, which includes the effects of composition in the MAX precursor, the combination of M-X elements, the synthesis route, and the desired form of MXenes (powder, clay, or single flakes). Next, we predict trends in the mechanical behavior of various compositions of MXenes based on relevant binary carbide literature and analyze the existing literature on the effect of composition and synthesis on the mechanical properties of MXenes. We then provide an in-depth perspective analysis of the state of experimental and predictive literature on MXenes' tribological performance as a (solid lubricant, lubricant additive and reinforcement phase). Lastly, we survey recent advances in MXenes to provide outlook for MXenes' future as a mechanical and tribological nanomaterial. This perspective study will provide a framework to analyze which compositions or forms of MXenes may be best in different applications to achieve desired mechanical and tribological properties.

2. Effect of MXene Synthesis on MXenes' Structure

Overall, MXenes' synthesis depends greatly on their MAX precursor. The M, A, and X composition of the MAX precursor is considered to be the key parameters which influences the ability and methods available to synthesize MXenes. The M-A bonds in MAX are metallic in nature,[13] but are predicted to be 3 - 4 times less stiff than the mixed ionic/covalent M-X bonds.[46] The metallic M-A bonds imply that MAX phases cannot be broken through traditional mechanical exfoliation, similar as graphite to graphene.[47] However, the use of top-down selective etching can break the weaker M-A bonds by the

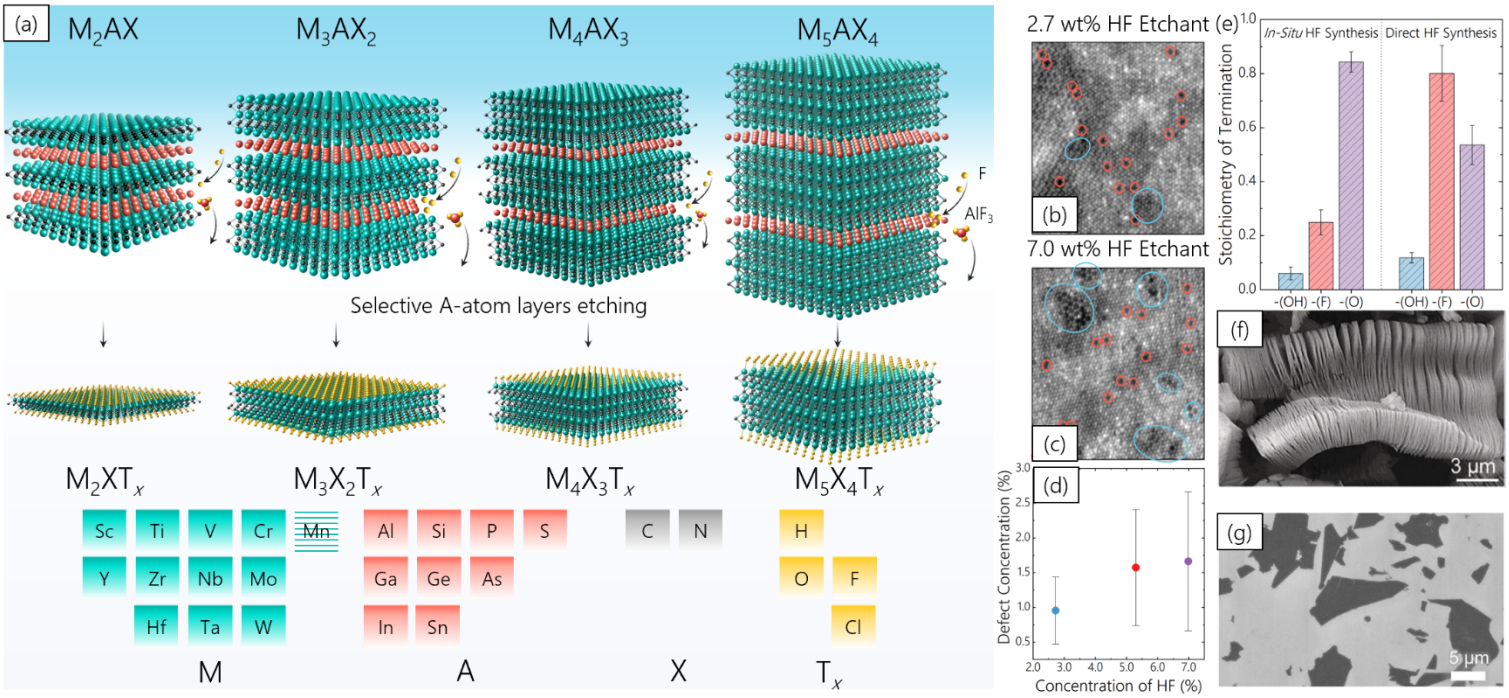

Figure 2. The HF-based synthesis of MXene from their MAX precursor and its effects on as well as various forms of MXene. (a) A schematic representation of MAX structures from n = 1 - 4 and their etched MXene structures with transition metals, carbon/nitrogen, the majority of A-group elements, and surface terminations. The solid gradient represents the compositions currently known in synthesized MXenes. The horizontal bars for Mn imply that Mn is only known in MAX precursors and has not yet been synthesized to MXene. (b-d) An increasing concentration of HF etchant is shown to increase the number of M vacancies in $Ti_3C_2T_x$ MXenes. Adapted with permission. [37] 2016, American Chemical Society. Red circles represent single M vacancies and blue circles indicate M vacancy clusters. The defect concentration is plotted in (d).[5, 6] (e) The composition of surface terminations is tunable by etchant, for which lower HF concentration made by in situ reaction of LiF and HCl result in higher $-O_2$ terminations as compared to higher $-F_2$ terminations for direct 48 % HF etching [11]. (f) HF used to etch MAX phases results in removed A layers from MAX to form exfoliated MXene particles. Reproduced with permission. [17] John Wiley & Sons, 2013. (g) The use of intercalant ions/molecules can delaminate MXenes into monolayers with lateral dimensions up to 10 μm. Reproduced with permission. [20] John Wiley & Sons, 2020.

removal of A-group elements and derive MXene from MAX. [13, 48] The parameters of this top-down selective etching process will affect the structure of MXene, which will majorly impact their resulting mechanical and tribological properties. A schematic representation of possible MAX structures and their etched MXene structures,[49] as well as the possibilities for transition metals,[14, 50, 51] carbon/nitrogen, majority of A-group elements in MAX phases,[21] and surface terminations of MXenes are shown in Figure 2a.

The process conditions for MXenes' selective etching are defined by etchant type, etchant concentration, etching temperature and duration, as well as environment. The combination of these parameters control MXenes' defects and surface terminations. In general, harsher conditions can create more defects.[5] The choice of the respective etching conditions depends on the type of the MAX precursor. Firstly, the A-group element in the MAX precursor affects what chemical etchants can be used for their successful exfoliation into MXenes, such as acid etching for A-group elements Al [13] and Si [52] or molten salt etching for A-group elements such as Al, Si, Ga and Zn.[53-55] Secondly, the energy required to exfoliate MAX to MXene decreases with a higher degree of reactivity (left-most side of the periodic table) of the transition metal in contact with A-group elements.[46] Therefore, MAX-phases with transition metals such as Cr, Mo, and W bonded to A-group elements necessitate harsher etching conditions for their successful exfoliation to MXene as compared to Ti, Zr, and Hf. In general, the use of harsher etching conditions tends to have an increased number of atomic vacancies.[5] This means that the A-group element in a MAX phase will affect the defect concentrations in two main ways. First, the A-group element in the MAX precursor will determine the chemical etchants which can be used to exfoliate MAX into MXene. Second, A-group elements having a significantly lower M-A bond energy than M-X and M-M (in Ti_3AlC_2, the M-X (Ti-C) is up to ~2.2 eV higher than the M-A (Ti-Al) bond energy) are more likely to have a lower concentration of defects than those with closer bond energies (such as Ti_3GeC_2 which has a difference of ~1.6 eV between the M-X (Ti-C) and M-A (Ti-Ge) bond energies).[46] In addition, the bond energy of M-C is generally higher than the bond energy of M-N for most transition metals (excluding Sc and Y).[56] This suggests that exfoliated transition metal carbide MXenes tend to have a lower concentration of atomic vacancies due to

selective etching than their nitride MXene counterparts. This is in agreement with previous studies, which identify the difficulty of the successful synthesis of $Ti_4N_3T_x$ MXene via traditional aqueous etching.[54]

$Ti_3C_2T_x$ MXene has been successfully synthesized via two main synthesis routes: aqueous hydrofluoric acid (HF) etchants [18, 48, 57] and Lewis acidic molten salt etchants.[53] While research is yet to investigate the effect of molten salt etching on the atomic defects in synthesized MXenes, it is known that the use of harshly acidic HF creates atomic vacancies in the synthesized MXenes.[5] HF etching of MXene has used HF concentrations between 5 to 48% either by the direct use of HF,[18, 57] or *in-situ* formed HF when utilizing lithium fluoride and hydrochloric acid (LiF/HCl) in molar ratios of LiF to MAX ranging from 5:1 to 12:1.[48] Increased HF concentrations tend to create higher concentrations of transition metal defects, (Figure 2b-d) and smaller flake sizes.[5, 18] However, to date, only concentrated HF has been used to synthesize non-titanium MXenes, while concentrations varied from 5% HF for Ti_2AlC to Ti_2CT_x [34] to 50% HF for Mo_2TiAlC_2 to $Mo_2TiC_2T_x$.[34] The composition of the surface terminations on MXene highly depends on the etching route, while higher HF concentrations result in more –F terminations as compared to –O or –OH terminations, as illustrated in Figure 2e.[11] Generally, the composition of the surface termination also depends on the type of M as well as M vacancies in MXenes, as Mo_2CT_x is shown to have a large amount of $-O_2$ terminations, while $Mo_{1.33}CT_x$ has more $-F_2$ terminations.[58]

After selectively removing the A-group elements from the MAX phase, MXenes can be used as a powder, in which MXene multi-layers are held together in a particle form as shown in Figure 2f.[17] However, MXene multi-layer powder can be further spaced apart with the use of intercalants such as Li^+, Na^+, water, or organic molecules.[28, 59] The behavior of MXene powders changes with the use of intercalants and works similar to clay.[48] For instance, the use of LiF/HCl etching of Ti_3AlC_2 to $Ti_3C_2T_x$ is shown to greatly increase the interlayer distances after etching by up to 7 Å as indicated by X-ray diffraction (XRD).[48] $Ti_3C_2T_x$ clay synthesized by LiF/HCl method is highly moldable, and can be rolled to form films with a high tensile strength up to 568 ± 24 MPa and conductivity as high as 15,100 $S \cdot cm^{-1}$,[27] which is impressive for one-step rolled films consisting of 2D nanosheets.

Further use of intercalants can delaminate MXenes into few- to single-flakes, as shown in Figure 2g, using Li-containing salts (LiF, LiCl) or organic molecules such as dimethyl sulfoxide (DMSO),[18] tetramethylammonium hydroxide (TMAOH),[18] tetrabutylammonium hydroxide (TBAOH),[18] or sonication.[60] The delamination process affects the number of defects and flake size, which, in turn, change MXenes' properties. Delamination methods, which use positively charged ions, such as Li^+ from the LiF/HCl exfoliation [38] or Li^+ ions added after HF exfoliation through the dissolution of Li-containing salts such as LiCl,[34] have led to larger lateral flake sizes (3 - 12 μm) with a lower defect density.[27, 61] Other methods require larger intercalation molecules such as DMSO, TBAOH, and TMAOH with prolonged mixing and sonication times, which typically result in smaller flake sizes (<1 μm) with a notable increased defect density.[18, 61, 62]

3. Mechanical Behavior of MXenes

The mechanical properties of MXenes are fundamental for their efficient use in nearly all applications, (Figure 1b) but are yet to be fully explored and understood. MXenes' specific combination of the M-X elements (M-C or M-N), surface terminations (M-O, M-OH, M-F, or M-Cl), and structure determines their mechanical properties.[63, 64] Currently, density functional theory (DFT) and molecular dynamics (MD) studies have been conducted on a significant array of MXenes,[2, 3, 4, 10, 29, 63-65, 66, 67, 68, 69, 70] but these studies still only represent a limited range of predictions as compared to the near limitless number of compositions.[49] This highlights the necessity for essential principles to guide the understanding of MXenes' mechanical behavior. In this section, we focus on the underlying behavior of M-X and M-T_x interactions in the structures of MXene. After discussing this behavior, we combine this analysis with the existing knowledge of predictions and experiments regarding the mechanical properties of MXene to recommend future directions on studies of the mechanical performance of MXenes.

At their most fundamental level, MXenes owe their mechanical behavior to the specific combination of M and X elements. While there are limited studies on MXenes' mechanical properties, the wealth of literature on 3D crystalline binary transition metal carbides/nitrides [71] can guide us in understanding the properties of MXene. Since C and N occupy similar octahedral, interstitial sites in MAX and MXenes [15, 21, 72, 73] and the (00ℓ)-planes in their hexagonal close-packed structure are similarly packed as the (111)-planes of the M-X rock-salt structures, our literature search first focused on 3D crystalline binary carbides and nitrides to bridge the current research gap in the understanding of the bonding strength of all possible M-X combinations.

In general, the bonding of transition metals to carbon or nitrogen is a mixture of ionic, covalent, and metallic bonding [74] and is owed to *d* and *s* electron orbitals of the transition metals [75], and the *p*-orbitals of C/N.[56] The ionic bonding between donated electrons

from M to X is theorized to act in tandem with the covalent bonding to form the primary bonds in the M-X structure.[76] Covalent bonding in transition metal carbides and nitrides is a mix of σ and π bonds, which depend on the geometry of the transition metal carbide/nitride crystal structure.[73, 77] The effects of X-X bonding are nearly negligible in the overall structure, as large distances between X-X result in considerable weak interactions,[74] which has been observed experimentally in the preferential evolution of methane gas during MXenes' hydrolysis.[78] The metallic bonding between the transition metals occurs via *d*-orbitals, which are not shared with carbon or nitrogen.[73] However, this metallic bonding between M-M contributes less to the lattice bond energy than M-X bonds.[74] In a reference frame of a singular octahedra M_6X structure (using X as the center atom), four of six of the inward-facing *d*-orbitals of M interact directly with X, while only two are antibonding orbitals and solely interact with other transition metals.[73] Additionally, the effect of carbon/nitrogen deficiencies increases the effect of the metallic bonding and decreases the effect of ionic/covalent M-X bonding in the overall lattice bond energy.[73, 79]

More specifically, the strength between M-X bonds can be characterized through the bond stiffness, which is derived from the bond energy and the M-X bond length. The bond stiffness can be used as a relation to the theoretical mechanical properties, such as Young's modulus.[80] We approximated the M-X bond length by using the length of a single covalent σ-bond between M and X.[81] Our approximation of the bond length between M and X based on single covalent bonds distance was verified when we compared this bond length to the bond distance of M-X in binary carbides and theoretical studies on MXenes in Table S1 and S2 (Supporting Information). Our analysis illustrated in Figure 3a indicates that the bond stiffness between M-C tends to increase with an increasing group number of M used in transition metal carbides. Furthermore, the bond stiffness of M-C tends to increase as the *d*-block order increases. Ti, Mo, and W tend to have the highest stiffness in M-C bonds in the 3*d,* *4d*, and 5*d* transition metal blocks of MXenes, respectively. In *3d*-block, Mn-C has a higher bond stiffness between M-C than Ti-C, however, Mn-C has only been synthesized in MAX phases and Mn-containing MXenes have not been made yet.[50]

In contrast, the bond stiffness between M-N bonds is slightly more complex than that of M-C bonds. In general, the M-N bond stiffness is maximized in the 3*d* block of transition metals. Additionally, these results indicate that Ti-N is likely to be the stiffest bond of all M-X pairs in MXenes. The tendency for M-N to have enhanced mechanical properties than M-C in bulk form for the 3*d*-block of transition metals can be confirmed through the comparison of the elastic moduli of 3D crystalline binary transition metal carbides and nitrides.[82] Specifically, at 637 GPa, the elastic modulus of TiN binary 3D phase is 1.4 times that of TiC, at 460 GPa,[83] while our analysis predicts the bond stiffness of Ti-N to be 1.2 times that of Ti-C. The increased stiffness of M-N over M-C bonds in earlier 3*d*-block transition metals and earlier group transition metals of the 4*d* and 5*d* blocks can be attributed to the additional available electron for bonding in nitrogen to the *d*-orbitals of the transition metal as compared to carbon.[84] The bond energy and stiffness of M-C and M-N are summarized in Table S3. Additionally, the equation used to calculate bond stiffness is shown in Eq. S1.

After establishing our bond stiffness predictions for various M-X pairs, we compared these predictions to the existing theoretical simulations of the 2D stiffness of bare MXenes (without surface terminations) [4, 29, 64, 65, 66] (Figure 3b and c) and terminated MXenes (Figure 3d). To date, the mechanical properties of M_2X MXenes are the most investigated ones across a wider range of transition metals and carbon/nitrogen,[3, 4, 63, 64, 65, 67] which allowed us to best compare our wide range of M-X bond combinations to currently published results. It is important to note that the 3D bulk elastic modulus of MXene (Figure 3e) is a different notation of mechanical stiffness than that of the 2D in-plane stiffness (Figure 3d), but is relatable by the monolayer thickness.[2, 3, 4] In general, an increasing monolayer thickness decreases the 3D bulk elastic modulus. Specifically, while surface terminated MXenes are predicted to have a comparable 2D stiffness to bare MXenes,[70, 85] surface terminations have been predicted to decrease the elastic modulus as compared to bare MXenes. This decrease in the elastic modulus is not based on fundamental changes in M-X interactions but is related due to an increased monolayer thickness due to existing surface terminations. Therefore, our approach focused on the 2D stiffness, as this analysis assists us in the identification of the effects of changing chemistry and compositions on the fundamental M-X structure of MXenes. The monolayer thicknesses of M_2CT_x and M_2NT_x are shown in Table S4 and S5, respectively. The equation used to relate the 3D elastic modulus and the 2D stiffness is shown in Eq. S2. The average 2D stiffnesses displayed in Figure 3d are shown in Table S6 and S7 for M_2CT_x and M_2NT_x, respectively.

Our systematic analysis of the bond strength between studies on binary transition metal carbides and nitrides provides insights into the likely mechanical properties' trend of different M and X compositions of MXenes. However, in all binary transition metal carbides and nitrides, the presence of C/N vacancies (lower concentration of X to M) tends to lower the mechanical properties of the bulk form.[82] Since MXenes are a few-

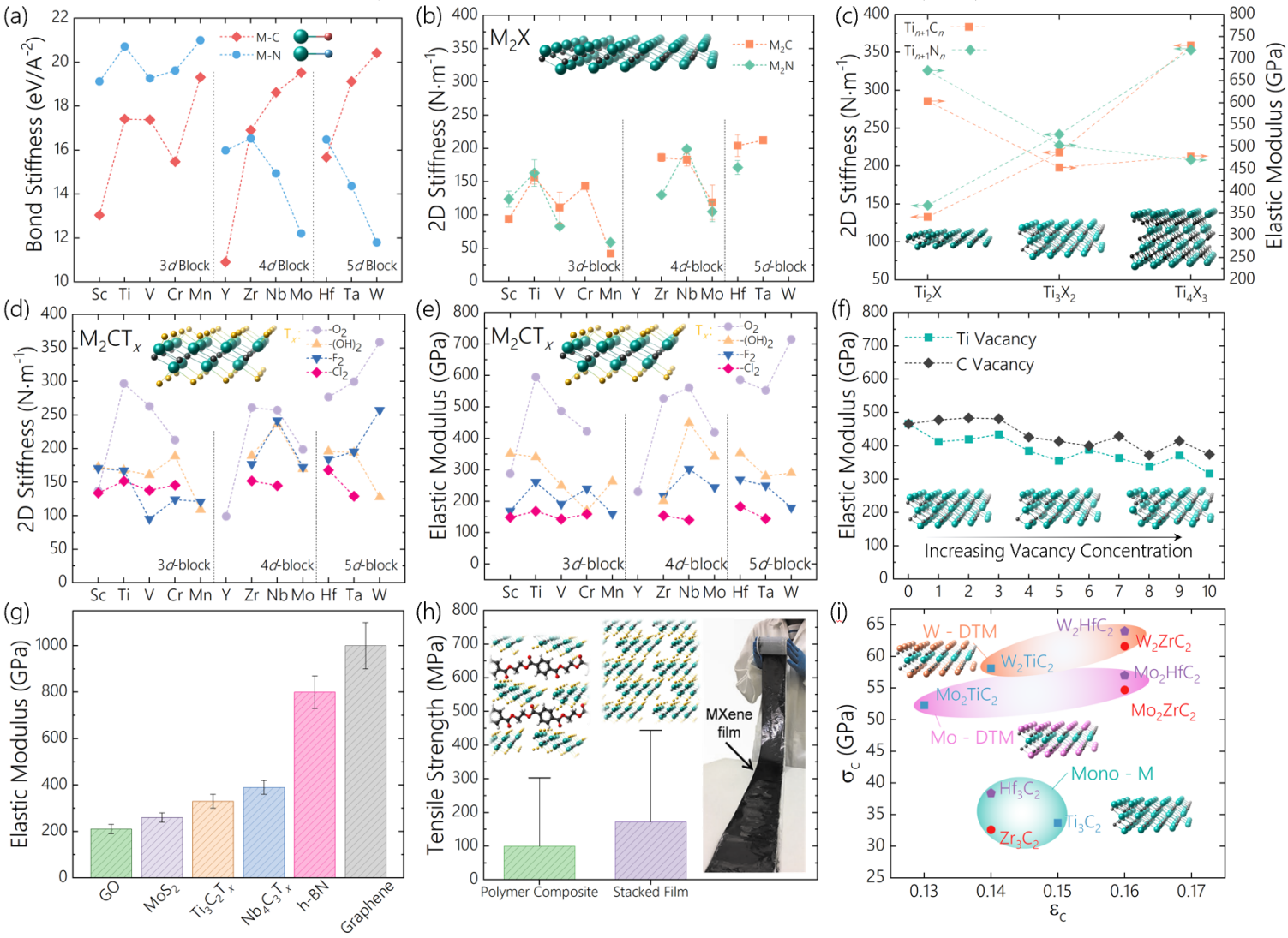

Figure 3. Theoretical and experimental mechanical behavior of MXenes. (a) Calculated bond stiffness between M-X for all early transition metals in an example rock-salt structure, for which orange diamonds represent M-C and blue circles represent M-N. (b) Average of all predictions on the mechanical stiffness of bare M_2X MXenes to date, related by monolayer thickness [2, 3, 4]. Bars represent average deviation of all predictions from the mean. (c) 2D stiffness and elastic modulus of $Ti_{n+1}X_n$ (X = C, N) MXene, which illustrate the effect of increasing flake thickness (n) on MXenes' mechanical stiffness. (d) Predictions on the mechanical 2D stiffness for terminated M_2XT_x MXenes for different surface terminations including $-O_2$, $-F_2$, $-(OH)_2$, and $-Cl_2$. (e) Prediction of the elastic modulus of terminated MXenes, which illustrates the effect of increased monolayer thickness due the surface terminations on the stiffness trends in MXene. (f) Effect of Ti and C vacancies on the 3D elastic modulus of $Ti_3C_2O_2$ MXene.[10] (g) The experimental elastic moduli for $Ti_3C_2T_x$ [16] and $Nb_4C_3T_x$ [19] MXenes as compared to other 2D nanomaterials. Adapted with permission [19]. Elsevier, 2019. (h) The averaged tensile strength of experimental tensile tests on $Ti_3C_2T_x$ MXene films with polymer composites (>80 wt.% $Ti_3C_2T_x$) [22, 23] or stacked $Ti_3C_2T_x$ MXene films.[22, 24-26, 27] Bars represent the standard deviation amongst all reported data, and data is further reported in Table S10. (i) Double transition metal MXenes with outer layers of Mo or W and interior layers of M = Ti, Zr, or Hf are stronger than their mono-M $M_3X_2O_2$ (M = Ti, Zr, Hf) counterparts. Adapted with permission [29]. Royal Society of Chemistry, 2018.

atom-thick flakes 2D material, they have two exterior atomic layers of transition metals which are not bonded to C or N at the surface.[6] Therefore, we must consider the effects of these outer layer transition metals with regards to their mechanical behavior. In binary carbides and nitrides, C/N deficiencies result in decreased M-X bonding and increased M-M bonding in the M-X structure, which decreases the overall bond strength of the lattice structure,[73] and further reduces the resulting mechanical stiffness as compared to structures without C/N deficiencies.[79, 82, 86]

Due to the likely effect of increased M-M interactions at the surface layer of MXenes, we expect the mechanical properties of MXenes will be lower than that of binary transition metal carbides and nitrides. This theory is supported by the stiffness predictions of $Ti_{n+1}C_n$ MXenes shown in Figure 3c, which show that an increasing MXene flake thickness result in increased 2D stiffnesses.The lower 2D stiffness in Ti_2C is due to the higher surface bonding interactions between Ti-Ti in the Ti_2C structure as compared with Ti_3C_2 or Ti_4C_3, which have more interior layers of Ti-C bonding without the

effect of surface Ti-Ti bonding. The decreased effect of the M-M surface layer bonding in thicker MXenes can be identified through the increase in 2D stiffness of $Ti_{n+1}C_n$ MXene as n increases, with 2D stiffnesses of 112.9 Nm^{-1}, 258.2 Nm^{-1}, and 323.3 Nm^{-1} for n = 1, 2, and 3, respectively.[4] This trend can also be seen for $Ti_{n+1}N_n$ MXenes, as the 2D stiffnesses are 118.4 Nm^{-1}, 241.9 Nm^{-1}, and 353.3 Nm^{-1} for n = 1, 2, and 3, respectively.[4] Although a recent MD study using a ReaxFF interatomic potential has predicted a different trend in 2D stiffnesses, with Ti_2CO_2 higher than $Ti_3C_2O_2$ at 604 $N{\cdot}m^{-1}$ as compared to 399 $N{\cdot}m^{-1}$ respectively,[10] this could be due consideration of $-O_2$ surface terminations and and/or ReaxFF's ability to reform broken covalent bonds in the M-X structure during failure [87], which has not been accounted for in previous simulations. In general, more studies are needed to fully understand the effect of M-M bonds, MXene structures, and surface terminations on their 2D stiffness.

In addition, the significantly lower 2D stiffness of Mo_2C (Figure 3b) compared to the predictions for the Mo-C bonds (Figure 3a) can be explained by the increased bonding interaction between Mo-Mo in thinner MXenes (n = 1). In Mo-containing MXenes, a change in n from 3 to 2 (M_4C_3 to M_3C_2) increases the Mo-Mo bond stiffness from 2.57 to 2.71 $eV/Å^{-2}$, while the Mo-C bond stiffness decreases from 8.19 to 7.84 $eV/Å^{-2}$.[46] This affinity towards M-M bonding is seen in transition metals such as Cr, Mo, and W in previous work investigating metal dimers and binuclear complexes.[88] This may indicate that carbide MXenes of transition metals Cr, Mo, and W with increased stiffnesses will be seen in thicker MXene structures (M_4C_3), for which the M-M bonding interaction decreases. In general, further analysis is necessary to determine the potential effects on the mechanical properties of thicker MXenes.

After evaluation the trends of M-X bonding in MXenes, we next look into the effect of different surface terminations on the mechanical properties of MXenes.[15] The bond energy of M-T_x tends to be maximized in the early transition metal groups (group 4), which has been explained as a combination of the propensity towards electron donation from the surface terminations (halides) to mostly unfilled *d*-orbitals of the surface early transition metal groups and an effect of the decreasing difference in electronegativity between the surface terminations and transition metals in the later transition metal groups (groups 5 and 6).[89, 90, 91] In general, $-O_2$ terminations result in a higher 2D stiffness of MXene, while $-F_2$, $-(OH)_2$, and $-Cl_2$ terminations either result in minor stiffness increases or no effects (Figure 3d). The effect of different surface terminations on the mechanical properties [2, 3, 67, 68, 69] can be explained by their effect on the M-X structure.[70] In $M_{n+1}X_n$ structures, the addition of strong mixed ionic/covalent M-O bonding reduces the contribution of M-M interactions,[89, 92] which serves to increase the M-X bond strength.[73] However, the mainly ionic bonding of M-F, M-Cl, or M-(OH) does not result in the same decrease in the M-M interactions for the $M_{n+1}X_n$ structure as compared to the M-O bonding. An exception can be found in $-Cl_2$ terminations on later group transition metals as a result of covalent bonding due to longer M-Cl bond lengths comparing to M-F bond lengths and an increased ionization energy for rightward transition metals in the periodic table.[91] This could explain the similar mechanical properties of V_2CCl_2 and Cr_2CCl_2 as compared to changes from V_2CF_2 and Cr_2CF_2 (Figure 3d).

In our analysis, we use the 2D stiffness to evaluate the effects of M, X, and T_x on the actual bond characteristics in MXenes' structure. In structural applications, the 3D elastic modulus is necessary to characterize the mechanical response of MXenes under loading conditions. The 3D elastic modulus is related to the 2D stiffness by the monolayer thickness, which adds an additional variable to the process. Additionally, all calculated 3D elastic modulus values based on the conversion in Eq. S2 are shown in Table S8 and S9 for M_2CT_x and M_2NT_x, respectively. As previously explained, an increase in n of $Ti_{n+1}X_n$ is shown to increase the 2D stiffness. However, the elastic modulus illustrates a different trend, as the elastic modulus decreases from 604 GPa to 454 GPa, and 479 GPa for n = 1, 2, and 3 in bare $Ti_{n+1}C_n$, respectively (Figure 3c). The effect of increased monolayer thicknesses of terminated M_2XT_x MXenes [3] on the elastic modulus is further seen in Figure 3e.

Experimental studies of the mechanical properties of monolayer MXenes have only been conducted on $Ti_3C_2T_x$ [16] and $Nb_4C_3T_x$ [19] demonstrating a 2D stiffness of 326 ± 29 Nm^{-1} and 486 ± 18 Nm^{-1}, respectively. These measured 2D stiffness values on single-flake MXenes agree with our discussion on the effect of transition metal composition (as shown in Figure 3a, and b that Ti-C is less stiff than Nb-C), and the increased n of $M_{n+1}X_n$ from 2 to 3 for $Ti_3C_2T_x$ and $Nb_4C_3T_x$, respectively. The lower values from the experimental measurements compared to the theoretical predictions for mechanical stiffness of MXenes (366 Nm^{-1} for $Ti_3C_2O_2$ and 605 Nm^{-1} for $Nb_4C_3O_2$ [3]) could be attributed to the presence of vacancies in the synthesized flakes, as vacancies significantly affect the properties of transition metal carbides and nitrides.[82] The elastic modulus of $Ti_3C_2O_2$ MXene for a vacancy concentration of 0% to 10% is illustrated in Figure 3f, which indicates the detrimental effect of vacancies on MXenes' mechanical properties.[10] Similarly, the presence of vacancies can explain the lower measured maximum

failure strength of MXenes compared to the predicted values. While the failure strength of $Ti_3C_2O_2$ has been predicted as 15.8% of the elastic modulus in theoretical studies,[10] the experimental failure strengths for $Ti_3C_2T_x$ and $Nb_4C_3T_x$ are only 5.2% and 6.8% of their elastic moduli, respectively.[16, 19] Additionally, synthesized MXenes have a mixture of surface terminations, instead of uniform -O_2 terminations, which can lower MXenes' stiffnesses and strengths.

Notably, the measured elastic moduli of $Ti_3C_2T_x$ and $Nb_4C_3T_x$ illustrates MXenes' status as the highest solution-processable nanomaterial to date, compared against common solution-processable 2D nanomaterials such as graphene oxide (GO) and MoS_2 and non-solution processable *h*-BN and graphene (Figure 3g).[19] As compared to only two studies on the mechanical behavior of single-flake MXenes, more studies on the mechanical properties of $Ti_3C_2T_x$ MXene films have been completed. In general, the mechanical properties of $Ti_3C_2T_x$ films are shown to be highly dependent on several parameters, including MXenes' flake size, their quality, the orientation of individual flakes of $Ti_3C_2T_x$, the film thickness, and the fabrication method,[24, 27] as displayed by the reported data in Figure 3h. The reported values for $Ti_3C_2T_x$ films are summarized in Table S10. For instance, a film made of randomly stacked $Ti_3C_2T_x$ layers resulted in tensile strengths as low as 40 MPa,[24] while highly oriented films, made by blade-coating, can result in tensile strengths as high as 568 MPa.[27] The change of film fabrication method from blade-coating to filtration reduced the tensile strength significantly.[27] An example of a blade-coated $Ti_3C_2T_x$ films with high tensile strength is shown in Figure 3h, which suggests blade-coating can be used for fabricating large-scale and high-strength MXene films.[27] Moreover, while $Ti_3C_2T_x$ MXene-polymer composite films have shown promise in different applications such as supercapacitors,[25] addition of polymers has been shown to reduce the mechanical properties of $Ti_3C_2T_x$ films, which can be due to the lower mechanical properties of the polymer, intercalated polymer chains and lack of primary bond formation between the polymers and $Ti_3C_2T_x$.[93] The research area of polymer-MXene composites requires more in-depth studies to gain knowledge on how to improve the mechanical properties of MXenes by polymer infiltration.

Future experimental studies on the mechanical properties of double transition metal MXenes can expand the possibilities to use MXenes where structural integrity is necessary. For instance, while Mo_2CT_x [94] or in-plane ordered divacancy MXene $W_{1.33}CT_x$ [95] have been synthesized, their thicker (n = 2 to 4) mono-transition metal MXenes are not available yet. Out-of-plane ordered double transition metals, as in experimentally synthesized $Mo_2TiC_2T_x$ and $Mo_2Ti_2C_3T_x$ [96] and theoretically stable $W_2M''C_3O_2$ (M″ = Ti, Zr, Hf),[29, 97] permits the use of these transition metals in higher n MXene structures. The use of Mo and W as M′ element in $M'M''C_3O_2$ (M″ = Ti, Zr, Hf) has been theoretically predicted to result in an increased mechanical strength by an average of 60% and 75% for Mo and W, respectively, over their mono transition metal counterparts $M_3C_2O_2$ (M = Ti, Zr, Hf), as shown in Figure 3i.[29]

Similarly, Mo containing thicker MXenes have been found in experimentally realized solid solution MXenes, such as $(Mo_{,}V)_4C_3T_x$ [98] and $(Mo_{,}V)_5C_4T_x$, [99] but their mechanical properties have not been tested yet. To date, the mechanical properties of carbonitride $M_{n+1}(C_{,}N)_n$ or solid solution MXenes $(M'_{,}M'')_{n+1}X_n$ have been theoretically investigated in a limited number of studies.[69, 100] It was suggested that by the addition of atoms with higher valence electrons in solid-solutions, the moduli can be increased, such as higher elastic constant in $Ti_{0.5}V_{1.5}C_2O_2$ compared to Ti_2CO_2.[69] This type of analysis has been conducted by previous investigations into the mechanical properties of mono-transition metal MAX phases.[100, 101] However, a systematic analysis of this type into the wide variety of carbonitride and solid solution MXenes is yet to be completed in theoretical studies and/or experimental analysis. Similarly, no mono-transition metal MXenes comprised of Sc or Y have been synthesized to date. However, these transition metals have been used to form in-plane ordered double transition metal MXenes, but these have yet to be mechanically tested experimentally.[102]

4. Tribological Behavior of MXenes

The wide possible compositions and forms of MXenes coupled with the low shear resistance between adjacent layers due to weak secondary inter-layer bonding make them particularly promising to be used for tribological purposes. In this section, we summarize the current understanding of MXenes as lubricant additives (Figure 4a), solid lubrication coatings (Figure 4b), as well as reinforcement phases in composites (Figure 4c). Additionally, we address the main challenges and future directions to boost MXenes' tribological performance, which are both connected to their tunable structures and their M-X and T_x compositions. DFT and MD studies assessing the tribological properties of MXenes revealed that the frictional properties between different layers depend on M-X composition, stoichiometry and surface terminations.[103-105] For Ti-based MXenes, low sliding pathways with coefficients of friction (COFs) of 0.24-0.27 and 0.10-0.14 were predicted for bare and terminated MXenes, respectively.[103] The importance of surface terminations was further confirmed through the assessment of the MXenes' sliding energy barrier. MXenes terminated with -O_2 illustrated reduced sliding

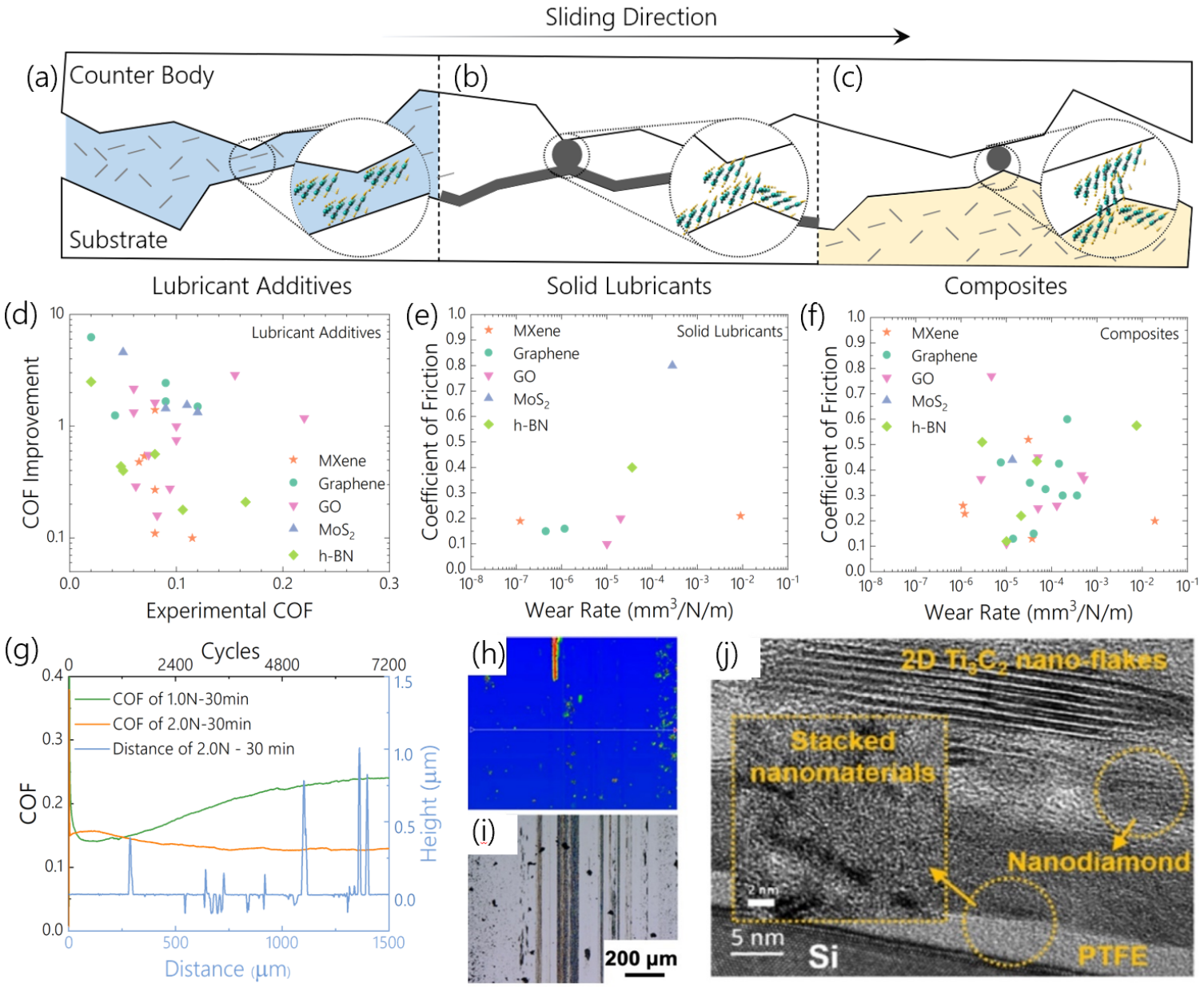

Figure 4. Tribological properties of MXenes. (a) Schematic illustration of their use as (a) lubricant additives, (b) solid lubricant coatings and (c) reinforcement phase in composites. (d-f) Evaluation of the tribological performance of MXenes when used as (d) lubricant additives (data in Table S11), (e) solid lubricants (data in Table S12) and (d) composites (data in Table S13) in comparison to other state-of-the-art 2D nanomaterials including graphene, graphene oxide (GO), MoS_2 and *h*-BN. (g) Evolution of the coefficient of friction (COF) of $Ti_3C_2T_x$/nanodiamond coating versus sliding distance for normal loads of 1 and 2 N and cross-sectional profile of the wear track, as well as the characterization of the resulting wear track by (h) white light interferometry, (i) light microscopy and (j) high-resolution transmission electron microscopy to elucidate the mechanisms of the involved tribo-film formation. Reproduced with permission [7]. Copyright American Chemical Society, 2019.

energy barriers by an order of magnitude compared to its bare counterpart (0.017 eV for Ti_2CO_2 versus 0.237 eV for bare Ti_2C), thus approaching energy barrier values of graphene (0.002 eV).[104] Terminated $Ti_3C_2T_x$ nanosheets were also shown to exhibit reduced binding energies compared to bare (no termination) sheets at the layers' interface.[105] The calculated values for MXenes point towards promising frictional, and possibly interesting wear characteristics, which may help to overcome important drawbacks of conventional solid lubricants.[106]

MXene multi-layer powders have been used as lubricant additives in paraffin [107], poly-(alpha)-olefins [108, 109] and other base oils [110, 111] to improve their friction and wear performance. COF reductions of up to 54 % and a 9-fold wear volume reduction have been verified for additive-free base oils with MXene concentrations of about 0.8-1.0 wt.%.[107, 108, 110-112] The worn surfaces were shown to be much smoother, less abraded and deformed, which was attributed to the formation of self-lubricating tribo-films and, therefore, enhanced load-bearing capacities. Increasing the MXene multi-layer particle

concentrations beyond the optimum values tend to increase friction due to potential agglomerations, thus lowering the dispersion's stability/quality and, consequently, resulting in downgraded tribological properties.[107] Similar results regarding the optimum concentration and wear features were obtained for MXenes/oxide hybrids, such as $Ti_3C_2T_x/TiO_2$ [111] and $Ti_3C_2T_x$/KTO [109] used as lubricant additives.

Recently, by the use of single- to few-layer $Ti_3C_2T_x$ flakes (delaminated MXenes) as additives in water, an improved friction and wear performance compared to multi-layer powder was reported. The maximum friction and wear rate reduction for $Ti_3C_2T_x$ flakes and multi-layer powder were measured to be 34 and 45 % as well as 10% and 5%, respectively. The larger increase for the single- to few-layer flakes were attributed to the ability to form MXene-rich self-lubricating tribo-films.[113] These values show the promise of single-flake MXene as a lubricant and possibly by the use of higher quality, larger flakes, and more stable $Ti_3C_2T_x$ MXene,[114] it can lead to further reduction in wear. As can be seen in Figure 4d, MXenes induce COFs between 0.06 and 0.1, but cannot yet reach the performance of other 2D nanomaterials in terms of absolute COF and factor of relative improvement. In this regard, the rationale manipulation of the surface chemistry may be an appropriate way to enhance their dispersion's stability thus further improving their performance as lubricant additives.

Solid lubricant coatings of MXenes have been deposited on various substrates by spray-coating or drop-casting and evaluated for their ability to reduce friction and wear. For contact pressures of about 0.57 GPa, 200-nm-thick $Ti_3C_2T_x$ MXene coatings on copper reduced the COF and wear rate by a factor of 4 and 10, respectively. This was explained by the formation of carbonaceous tribo-films as verified by Raman spectroscopy, which underwent sliding-induced graphitization thus ensuring beneficial friction and wear properties over time.[115] Drop-casted MXene coatings on stainless steel demonstrated a similar 3.5-fold friction reduction and pronounced changes in the underlying wear mechanisms under very dry conditions (relative humidity of 4 %).[116] Recently, the friction and wear response of drop-casted MXene coatings was studied as a function of relative humidity and contact pressure.[117] For high contact pressures of 0.80 GPa and low relative humidity of 20 %, MXene coatings induced a 2.3-fold friction reduction and a 2.7-fold wear volume reduction due to the formation of self-lubricating tribo-films of compacted MXenes. Inspired by these encouraging results, 3-µm-thick drop-casted MXene coatings were tested in higher loaded thrust ball bearings under applied axial loads of 130 N, a contact pressure of 0.8 GPa and 1000 RPM. A 3.2-fold reduction of the frictional torque and a 2.1-fold extension of the service life interval thus reaching 750,000 revolutions were achieved while keeping the frictional torque sufficiently low to ensure proper functioning.[118] Figure 4e highlights the excellent performance of MXenes' solid lubricant coatings with COFs of about 0.2 and wear rates on the order of 10^{-7} mm^3/Nm, which is comparable to the behavior of the other 2D nanomaterials. Considering the early stage of tribological research on MXenes, it can be envisioned that MXenes can induce even more beneficial effects thus making them the next-generation solid lubricant systems.

Atomic and friction force microscopy studies using multilayer powder as well as single- to few-layer MXene have demonstrated their overall ability to reduce friction at the nano-scale.[119, 120] $Ti_3C_2T_x$ MXenes etched via different routes (HF, HCl-LiF, and TMAOH delamination) demonstrated notable differences regarding their pull-off and slide-off forces as well as contact angles and work of adhesion, which were connected to the changes in their surface terminations.[120] Very recently, Nb_2CT_x MXenes have shown lower frictional and adhesive forces compared to $Ti_3C_2T_x$, which was connected to their different molecular structure thus inducing differences in the surface dipole moment densities.[121]

MXenes have been used as reinforcement phase in polymer composites to improve their mechanical and tribological properties.[122-126] Epoxy [123-126] and ultra-high molecular weight polyethylene (UHMWPE) [122] have been reinforced by either multi-layer powder,[122, 123] few-layer [124], chemically functionalized few-layer MXenes [126] or MXene/graphene [124] and MXene/carbon nanofiber hybrids.[125] The addition of MXenes slightly enhanced the mechanical properties (e. g., hardness, impact and flexure strength), thus inducing a 3-fold friction reduction in epoxy composites containing 2 wt.% $Ti_3C_2T_x$ MXene.[123] Epoxy composites reinforced by amino-functionalized few-layer $Ti_3C_2T_x$ MXene demonstrated ~ 35 % lower friction and 72 % reduced wear rate. This was ascribed to the improved dispersion and compatibility of the functionalized MXenes in the organic matrix, thus increasing the storage modulus and interfacial strength as well as reducing plastic deformation and microcracking.[126] This study ultimately demonstrated the potential of the MXenes' chemical functionalization to further boost their mechanical and tribological performance. Besides chemical functionalization, 3D $Ti_3C_2T_x$-epoxy composite architectures (1 wt.% $Ti_3C_2T_x$) fabricated by liquid phase blending and freeze dying demonstrated a 4-fold friction and 3-fold wear reduction (wear volume and rate) due to an improved interfacial strength and nano-sheets' alignment.[125] Finally, the usage of nano-hybrids as

reinforcement phase in composites, such as epoxy reinforced by graphene-wrapped few-layer MXenes, induced a friction and wear rate reduction of 10 and 89 %, respectively, which were better than the individual $Ti_3C_2T_x$ MXene or graphene (wear reduction by 52 and 69 %, respectively). This synergetic effect was attributed to the formation of self-lubrication tribo-films induced by both nanomaterials.[124] Although a detailed characterization of the formed tribo-film was not presented, this study unambiguously underlined the outstanding potential of MXene hybrids to improve friction and wear.

Copper [127] and aluminum composites [128, 129] have been reinforced by either multi-layer powder [128] or few-layer delaminated MXene flakes.[127, 129] Copper/MXene composite coatings reduced the COF and wear rate by a factor of 2 and 19, respectively, compare to pure copper,[127] while aluminum reinforced by multi-layer MXene powder demonstrated a 2.5-fold friction reduction compare to pure aluminum.[128] These effects were speculated to arise from the formation of self-lubricating MXene-rich tribo-film, which created an easy-to-shear interface and helped to reduce direct metal-metal contact.[127] Figure 4f underlines the excellent tribological performance of MXenes when used as reinforcement phase in polymeric and metallic composites with COFs of about 0.25 and wear rates on the order of 10^{-6} mm^3/Nm. Further improvements of the adhesion between the nanosheets and the matrix may lead to even more beneficial results.

MXenes' potential to improve friction and wear was recently demonstrated as hybrid coatings, such as MXene/nanodiamond and MXene/nanodiamond quantum dot hybrids, for solid lubrication.[7, 130] When rubbed against PTFE under low contact pressures, a higher wear resistance and reduced COFs for MXene/nanodiamond hybrids were demonstrated (Figure 4g). This hybrid led to an improvement in COFs by 46 % and 30 % compared to pure $Ti_3C_2T_x$ and nanodiamond coatings, respectively.[7] The study confirmed the formation of a nano-structured MXene-rich tribo-film by high-resolution transmission electron microscopy (TEM) (Figure 4h). The MXenes' ability to form long-lasting, wear-resistant tribo-films coupled with their enhanced interlayer bonding characteristics verifies MXenes' superior wear performance compared to other 2D nanomaterials. This can help to overcome important drawbacks of graphene and its derivates, which easily wear off once the first signs of wear have started to occur.[106]

Irrespective of the MXenes' usage as lubricant additive, reinforcement phase in composites or solid lubricant, many studies speculated that the formation of self-lubricating MXene-rich tribo-films is responsible for their excellent friction and outstanding wear performance. However, direct characterization to confirm the tribo-film formation is lacking. Recently, Yin et al. used high-resolution TEM on MXene hybrid coatings to confirm the existence of nanostructured MXene-rich tribo-films.[7, 130] Understanding of energy-dissipating friction and wear mechanisms of MXenes via high-resolution chemical, structural, and morphological characterization of the tribological interface and formed tribo-films is essential for the long-term low-friction and low-wear performance.

Due to local high temperatures and high contact pressures acting in a tribological contact the detailed study of the chemical and structural evolution of tribologically-stressed MXenes is essential to fully elucidate the underlying mechanisms. MXenes can degrade structurally (increased defect density, sheets bending/breakage, reduced lateral sheets size, among others) or chemically (oxidation, changed surface terminations, among others), which may certainly affect the tribo-film formation. Furthermore, the influence of tribo-chemical reactions with the involved counter-bodies and the environment (oxygen and water), which may lead to the preferred formation of certain oxide species depending on the acting temperature and pressure, need to be studied in detail. Consequently, well-designed tribological experiments coupled with advanced materials characterization are required to understand the contribution of these individual aspects (chemical and structural degradation as well as tribo-chemical reactions) on the tribo-film formation as well as the resulting macroscopic friction and wear performance.

In studies involving MXenes as lubricant additives, only ball-on-disk tribometry has been utilized to assess their tribological performance in additive-free base oils. As friction and wear are system-dependent properties, a simple change of the test-rig (pin-on-disk, four-ball tester, etc.) modifies the contact conditions, which could possibly induce more beneficial tribological effects. All studies published to date, made use of ultrasonication to mix MXenes with additive-free base oils. The MXene dispersion's stability and agglomerates' sizes, which both tend to change with time and MXenes' concentration, are crucial parameters to ensure beneficial tribological properties under lubricated conditions, but remained often unexplored in currently published studies. The MXenes' hydrophilic nature due to their surface terminations downgrades their dispersion's stability in apolar base oils. Therefore, one can use existing functional groups ($-O_2$, $-(OH)_2$, $-F_2$ and Cl_2) as anchoring points for hydrophobic molecules (e.g., longer hydro-carbon chains) to gradually manipulate their hydrophobic/hydrophilic properties. This, in turn, significantly improve the dispersion's stability in hydrophobic liquids and reduce the likelihood of MXenes

to agglomerate thus boosting the resulting frictional performance.

Considering solid lubrication coatings, deposition strategies to ensure uniform and homogeneous MXene coatings with optimized interfacial properties are yet to be developed. Chemically functionalized MXenes can be an excellent way to improve the substrate/coating adhesion, which could further boost the tribological performance of hybrids due to stronger surface interactions, as well as bonding possibilities with other 2D nanomaterials. Furthermore, additional work to assess the nano-tribological properties, such as frictional layer dependency, should be done using single-, bi-, few- and multi-layer MXenes as a function of surface terminations. These studies would ultimately assist in the clarification of the underlying energy-dissipating friction and wear mechanisms of MXenes at the nanoscale (puckering, electron-phonon interaction, among others). Additionally, nano-tribological studies need to consider the overall MXenes' quality, such as a correlation between the defect situation (type and density of defect) with friction and wear. As well, AFM and FFM measurements (sheet-on-sheet) should be conducted to study the interlayer friction thus verifying DFT and MD predictions.

In MXene reinforced composites, characterization of MXene matrix interface (chemistry, structure and morphology) by the use of high-resolution characterization techniques are needed, which is essential for the design of enhanced MXene/matrix interfacial strengths. In general, weak interfaces in composites is often considered as the "bottleneck" in composites, as it can lower the mechanical and tribological performances. Additionally, more research should be dedicated to the homogeneous MXenes distribution in the matrices with correlation to its effects on friction and wear. Ceramic matrix composites reinforced by MXenes are yet to be explored for tribological exploration, and are expected to be another potential field of application due to the inherent wear resistance of ceramics.

4. Recent Advances, Outlook, and Conclusion

The recent advances in the last few years on the synthesis and post-synthesis processes of MXenes can open up further opportunities for research into their mechanical and tribological properties. Figure 5 displays the effects of new synthesis routes on the fundamental chemistry and composition of MXenes, which can provide new methods to tune the resulting mechanical and tribological properties of MXenes for desired behavior. Figure 5a-c show examples of these newer synthesis methods, such as a combination of an aqueous HF and HCl (HF/HCl) wet-chemical etchant (Figure 5a),[131, 132] non-aqueous wet chemical etching process using NH_4HF_2 (Figure 5b),[133] and molten salt etching (Figure 5c).[53, 55] HF/HCl etching of MXene can be used to control the amount of HF necessary for the exfoliation process, which has shown to result in a lower defect density [132, 134] and improved electrical properties.[132] Non-aqueous etching of MXene results in solvents other than water, for which long-term storage of MXene in water has shown an overall decrease in electrical properties due to oxidation of MXene sheets.[135] Recent advances in the capping of MXene edges with poly-anionic salts have shown promise to prevent the oxidation of MXene flakes in aqueous solutions.[136] In addition, the use of excess Al in the synthesis of Ti_3AlC_2 showed an improved oxidation stability of the resulting MXenes[114] These methods to reduce atomic defects or detrimental oxide formation in MXenes permit the use of more pristine MXene sheets, as shown in (Figure 5d). Moreover, recent advances in molten salt etching provide new ways of etching A-group elements such as Si, Zn, and Ga,[53] which can open up doors to new transition metal compositions and structures of MXenes, which have not been synthesizable with Al (Figure 5e). Similarly, molten salt treatments of MXenes have induced either uniform or removed surface functionalities as well as have expanded the available termination chemistries (Figure 5f).[55]

These advances illustrate MXenes' ever-expanding potential as designable and tunable materials towards desired mechanical or tribological properties. The use of non-Al A-group elements in MAX phase synthesis could permit the formation of MXenes with a controllable 2D thickness in ranges of n = 1 to 4. The ability to control MXene thickness could be used to either increase the reactivity of the transition metals of MXenes for beneficial oxide formation at lower thicknesses (n = 1, 2) or to reduce the impact of the surface transition metal effect (Figure 3d) on the stiffness of MXenes for the mechanical performance for higher flake thicknesses of n = 3, 4 (Figure 5g). The possible variations in the 2D flake thickness, such as M_2XT_x to $M_5X_4T_x$, gives MXenes a unique advantage over other 2D materials as this permits study of primary bonds effects in structures with two to five layers of transition metals, interleaved with carbon or nitrogen atoms, on the mechanical properties.

The available methods of tuning of the mechanical stiffness of MXenes is also expanded by new available compositions in transition metals and surface terminations (Figure 5h). There is currently significant room for exploration of the mechanical properties of MXenes between the different transition metals and C/N compositions, the structures of $M_{n+1}X_nT_x$ (n = 1, 2, 3, 4), and the use of ordered and solid solution double transition metal MXenes. The existent theoretical and experimental studies on MXenes illustrate comparable behavior to well-explored binary transition metal carbides/nitrides, which allows for insight into the performance of different

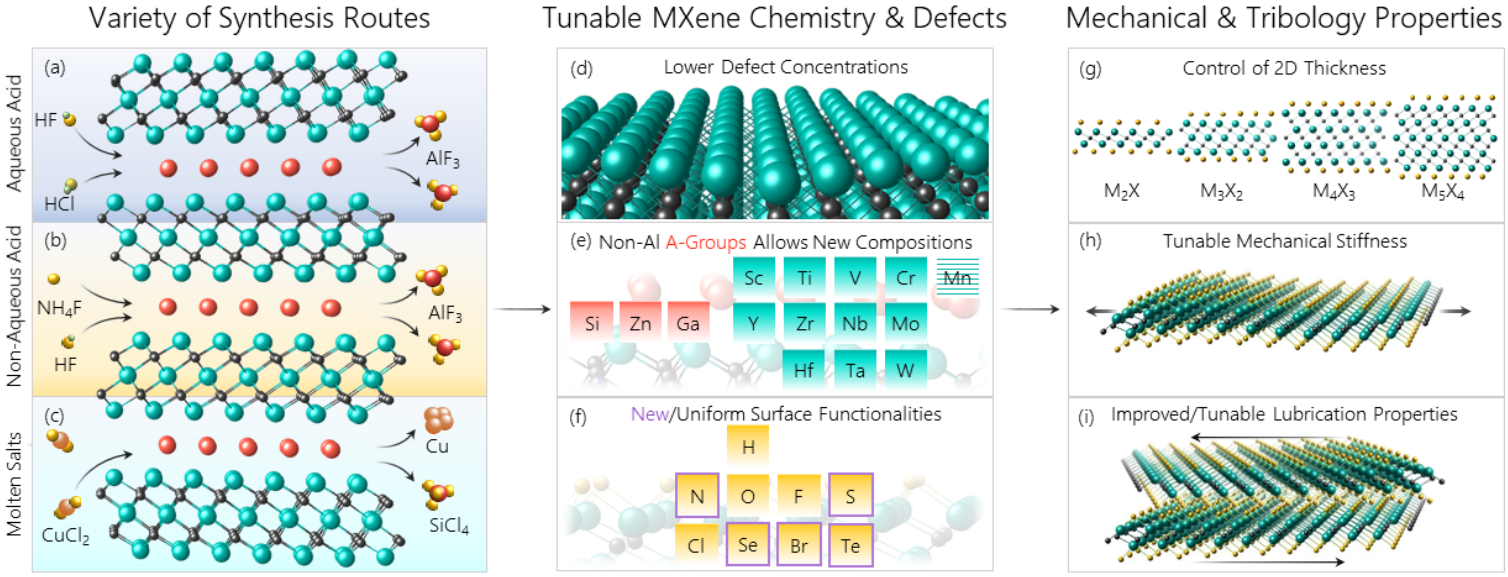

Figure 5. Recent advances in the synthesis routes of MXenes have expanded the tunability of the chemistry of MXenes towards improved mechanical and tribological applications. (a-c) Schematic of MXene synthesis routes, such as (a) mixed acids HF/HCl, (b) non-aqueous etching solutions, and (c) molten salt etching with some of their reactants and products shown. (d-f) Effect of these synthesis routes of MXene chemistry and defects, where these methods can be used to result in MXene flakes with (d) a lower defect density or (e) expand possible M or (f) T_x compositions. (g-i) The expansion in chemistries and compositions (g) provides new opportunities to design MXenes for (h) mechanical or (i) tribological purposes.

M-X compositions, the effect of M-X non-stoichiometry, the consequence of M and X vacancies, and the impact of surface terminations. We believe that fundamental understanding of MXenes mechanical behavior will allow tunable mechanical properties for a wide array of future applications, which is not seen in any other 2D nanomaterial. Additionally, as the mechanical properties of MXene lends considerable influence into the tribological properties of MXene, we believe the mechanical behavior tunability of MXenes will create considerable control over their tribological potential.

To date, the tribology studies on MXenes have mainly explored Ti-based MXenes (mainly $Ti_3C_2T_x$). MXenes' structural diversity and large compositional space lends possibilities for limitless research endeavors toward optimization of MXene for frictional and wear behavior. The recent advances in MXene synthesis provide new compositional options in transition metals and surface terminations could result in stronger MXenes for higher frictional durability and lower inter-layer sliding forces, respectively (Figure 5i). In addition, the ability to chemically functionalize MXenes, based upon their surface terminations, considerably enhance their dispersion's stability (additives) as well as adhesional and interfacial strengths (solid lubricants and composites). This will contribute to lower COFs and wear rates thus notably extending service life intervals and, therefore, the system's energy efficiency. MXene-based tribo-systems can potentially outperform graphene and its derivatives due to the formation of ultra-wear-resistant tribo-films. In order to make this promising and encouraging start a real success story, we emphasize that more fundamental research is necessary to explore the underlying friction and wear mechanisms.

In addition, MXenes variety of synthesis routes offer an exciting level of compositional control that is not seen in any other nanomaterial, which provides a fascinating new avenue for fundamental study of the mechanical and tribological behavior of 2D materials. Traditionally, the impact of local bonding and composition on the mechanical and tribological properties of materials is limited by the available methods of bottom-up synthesis. The ability to form 2D flakes of transition metal carbides and nitrides in a wide array of transition metal, C/N, and surface termination compositions via top-down synthesis methods permits comparative studies on the underlying principles of chemical bonding, atomic structures, and synthesis methods on the mechanical and tribological performance of transition metal carbide and nitride materials. Breakthroughs in the understanding of these principles can open the door toward atomic level engineering of MXenes for structural and low-friction bulk applications in films, hybrid, or composite materials.

In conclusion, MXenes have the highest stiffness among the solution-processed 2D materials. Additionally, the wide variety of compositions and MXene forms lends considerable possibilities for the mechanical and tribological behavior of MXenes. The entire current array of applications of MXene, which range from energy storage to biology, require fundamental understanding of the mechanical and tribological properties to fully identify their behavior. The recent movement toward large-scale synthesis of MXene further highlights the need for rapid acceleration of the fundamental

understanding of these crucial properties. In addition, the ability to use MXenes in different applications as thin-films, composite additives, or in liquid lubricants allows MXenes to function in many new applications, such as solution processable structural composites or triboelectric energy generators. The future applications for MXene is ever-expanding and potentially world changing, and we believe that the true realization of the potential of the entire MXene family requires the fundamental research of these necessary properties.

Conflict of Interest: The authors declare no competing financial interest.

Acknowledgments: BA and BCW acknowledge startup funding from the Department of Mechanical and Energy Engineering and Purdue School of Engineering and Technology at IUPUI. AR gratefully acknowledges CONICYT-ANID for the financial support given within the project Fondecyt 11180121 as well as the VID of the University of Chile in the framework of “U-Inicia UI013/2018”.

Brian C. Wyatt is a Ph. D. student in the layered materials and structures lab in the Mechanical and Energy Engineering department at Indiana University – Purdue University – Indianapolis. He received his Bachelor of Science degree in Mechanical Engineering at Rose-Hulman Institute of Technology in Terre Haute, IN in 2019. His current research focus is on the inclusion of MXenes into lightweight metals for bio-inspired structural application. His scientific interests include the mechanical characterization and composition control of two-dimensional nanomaterials as well as the investigation of their interfacial properties in structural composite materials. Brian can be reached by email at bcwyatt@iu.edu.

Andreas Rosenkranz is a Professor for Materials-oriented Tribology and New 2D Materials in the Department of Chemical Engineering, Biotechnology and Materials at the University of Chile. His research focuses on the characterization, chemical functionalization and application of new 2D materials. His main field of research relates to tribology (friction, wear and energy efficiency), but in the last couple of years, he has also expanded his fields towards water purification, catalysis and biological properties. He has published more than 100 peer-review journal publications, is a fellow of the Alexander von Humboldt Foundation and acts as a scientific editor for different well-reputed scientific journals including Applied Nanoscience and Frontiers of Chemistry.

Babak Anasori is an assistant professor at the Purdue School of Engineering and Technology at Indiana University – Purdue University Indianapolis. He received his Ph. D. degree in materials science and engineering from Drexel University in 2014. He is one of the inventors of ordered double-transition metal MXenes, as a result of his postdoctoral research. His current research focuses on the synthesis and characterizations of novel MXenes and their composite and their mechanical properties. He is currently the chair of the Early Career Professionals Subcommittee of the Materials Research Society.

References

[1] Q. Zhang, J. Q. Huang, W. Z. Qian, Y. Y. Zhang, F. Wei, Small 2013, 9, 1237; P. G. Bruce, S. A. Freunberger, L. J. Hardwick, J. M. Tarascon, Nat Mater 2011, 11, 19.

[2] Z. Fu, H. Zhang, C. Si, D. Legut, T. C. Germann, Q. Zhang, S. Du, J. S. Francisco, R. Zhang, The Journal of Physical Chemistry C 2018, 122, 4710; Y. Qin, X. H. Zha, X. Bai, K. Luo, Q. Huang, Y. Wang, S. Du, J Phys Condens Matter 2019, 32, 135302.

[3] T. Hu, J. Yang, W. Li, X. Wang, C. M. Li, Phys Chem Chem Phys 2020, 22, 2115.

[4] N. Zhang, Y. Hong, S. Yazdanparast, M. Asle Zaeem, 2D Materials 2018, 5.

[5] X. Sang, Y. Xie, M. W. Lin, M. Alhabeb, K. L. Van Aken, Y. Gogotsi, P. R. C. Kent, K. Xiao, R. R. Unocic, ACS Nano 2016, 10, 9193.

[6] B. Anasori, M. R. Lukatskaya, Y. Gogotsi, Nature Reviews Materials 2017, 2.

[7] X. Yin, J. Jin, X. Chen, A. Rosenkranz, J. Luo, ACS Appl Mater Interfaces 2019, 11, 32569.

[8] H. O. Navneet Sharma, Ambika Bharadwaj, Dharam Pal Pathak, Rakesh Kumar Sharma, RSC Advances 2015, 5, 53381.

[9] D. P. Dubal, Chodankar, N. R., Kim, D. H., & Gomez-Romero, P. , Chemical Society Reviews 2018, 47, 2065.

[10] G. Plummer, B. Anasori, Y. Gogotsi, G. J. Tucker, Computational Materials Science 2019, 157, 168.

[11] M. A. Hope, A. C. Forse, K. J. Griffith, M. R. Lukatskaya, M. Ghidiu, Y. Gogotsi, C. P. Grey, Phys Chem Chem Phys 2016, 18, 5099.

[12] Z. H. Lin, Xie, Y., Yang, Y., Wang, S., Zhu, G., & Wang, Z. L., ACS Nano 2013, 7, 4554.

[13] M. Naguib, M. Kurtoglu, V. Presser, J. Lu, J. Niu, M. Heon, L. Hultman, Y. Gogotsi, M. W. Barsoum, Adv Mater 2011, 23, 4248.

[14] Y. Gogotsi, B. Anasori, ACS Nano 2019, 13, 8491.

[15] C. Shi, M. Beidaghi, M. Naguib, O. Mashtalir, Y. Gogotsi, S. J. Billinge, Phys Rev Lett 2014, 112, 125501.

[16] A. Lipatov, Lu, H., Alhabeb, M., Anasori, B., Gruverman, A., Gogotsi, Y., Sinitskii, A., Sci Adv 2018, 4, 1.

[17] M. Naguib, V. N. Mochalin, M. W. Barsoum, Y. Gogotsi, Adv Mater 2014, 26, 992.

[18] M. Alhabeb, K. Maleski, B. Anasori, P. Lelyukh, L. Clark, S. Sin, Y. Gogotsi, Chemistry of Materials 2017, 29, 7633.

[19] A. Lipatov, M. Alhabeb, H. Lu, S. Zhao, M. J. Loes, N. S. Vorobeva, Y. Dall'Agnese, Y. Gao, A. Gruverman, Y. Gogotsi, A. Sinitskii, Advanced Electronic Materials 2020.

[20] A. Lipatov, M. Alhabeb, M. R. Lukatskaya, A. Boson, Y. Gogotsi, A. Sinitskii, Advanced Electronic Materials 2016, 2.

[21] M. Sokol, V. Natu, S. Kota, M. W. Barsoum, Trends in Chemistry 2019, 1, 210.

[22] W. Tian, A. VahidMohammadi, M. S. Reid, Z. Wang, L. Ouyang, J. Erlandsson, T. Pettersson, L. Wagberg, M. Beidaghi, M. M. Hamedi, Adv Mater 2019, 31, e1902977.

[23] W. T. Cao, F. F. Chen, Y. J. Zhu, Y. G. Zhang, Y. Y. Jiang, M. G. Ma, F. Chen, ACS Nano 2018, 12, 4583.

[24] K. L. Firestein, J. E. von Treifeldt, D. G. Kvashnin, J. F. S. Fernando, C. Zhang, A. G. Kvashnin, E. V. Podryabinkin, A. V. Shapeev, D. P. Siriwardena, P. B. Sorokin, D. Golberg, Nano Lett 2020.

[25] Z. Ling, C. E. Ren, M. Q. Zhao, J. Yang, J. M. Giammarco, J. Qiu, M. W. Barsoum, Y. Gogotsi, Proc Natl Acad Sci U S A 2014, 111, 16676.

[26] S. Luo, S. P. Patole, S. Anwer, B. Li, T. Delclos, O. Ogogotsi, V. Zahorodna, V. Balitskyi, K. Liao, Nanotechnology 2020; L. Ding, Y. Wei, L. Li, T. Zhang, H. Wang, J. Xue, L. X. Ding, S. Wang, J. Caro, Y. Gogotsi, Nat Commun 2018, 9, 155.

[27] J. Zhang, N. Kong, S. Uzun, A. Levitt, S. Seyedin, P. A. Lynch, S. Qin, M. Han, W. Yang, J. Liu, X. Wang, Y. Gogotsi, J. M. Razal, Adv Mater 2020, e2001093.

[28] X. Wang, X. Shen, Y. Gao, Z. Wang, R. Yu, L. Chen, J Am Chem Soc 2015, 137, 2715.

[29] Z. Fu, S. Zhang, D. Legut, T. C. Germann, C. Si, S. Du, J. S. Francisco, R. Zhang, Phys Chem Chem Phys 2018, 20, 29684.

[30] K. Hantanasirisakul, M.-Q. Zhao, P. Urbankowski, J. Halim, B. Anasori, S. Kota, C. E. Ren, M. W. Barsoum, Y. Gogotsi, Advanced Electronic Materials 2016, 2.

[31] C. J. Zhang, B. Anasori, A. Seral-Ascaso, S. H. Park, N. McEvoy, A. Shmeliov, G. S. Duesberg, J. N. Coleman, Y. Gogotsi, V. Nicolosi, Adv Mater 2017, 29.

[32] S. J. Kim, H. J. Koh, C. E. Ren, O. Kwon, K. Maleski, S. Y. Cho, B. Anasori, C. K. Kim, Y. K. Choi, J. Kim, Y. Gogotsi, H. T. Jung, ACS Nano 2018, 12, 986; K. Montazeri, M. Currie, L. Verger, P. Dianat, M. W. Barsoum, B. Nabet, Adv Mater 2019, 31, e1903271.

[33] T. Yun, H. Kim, A. Iqbal, Y. S. Cho, G. S. Lee, M. K. Kim, S. J. Kim, D. Kim, Y. Gogotsi, S. O. Kim, C. M. Koo, Adv Mater 2020, e1906769; A. Iqbal, Shahzad, F., Hantanasirisakul, K., Kim, M.K., Kwon, J., Hong, J., Kim, H., Kim, D., Gogotsi, Y., Min Koo, C., Science 2020, 369, 446.

[34] M. Han, C. E. Shuck, R. Rakhmanov, D. Parchment, B. Anasori, C. M. Koo, G. Friedman, Y. Gogotsi, ACS Nano 2020, 14, 5008.

[35] X. Wu, Z. Wang, M. Yu, L. Xiu, J. Qiu, Adv Mater 2017, 29; X. Zang, W. Chen, X. Zou, J. N. Hohman, L. Yang, B. Li, M. Wei, C. Zhu, J. Liang, M. Sanghadasa, J. Gu, L. Lin, Adv Mater 2018, 30, e1805188.

[36] H. Huang, J. Cui, G. Liu, R. Bi, L. Zhang, ACS Nano 2019, 13, 3448; R. Meng, J. Huang, Y. Feng, L. Zu, C. Peng, L. Zheng, L. Zheng, Z. Chen, G. Liu, B. Chen, Y. Mi, J. Yang, Advanced Energy Materials 2018, 8.

[37] R. B. Rakhi, P. Nayak, C. Xia, H. N. Alshareef, Sci Rep 2016, 6, 36422.

[38] A. Levitt, J. Zhang, G. Dion, Y. Gogotsi, J. M. Razal, Advanced Functional Materials 2020.

[39] K. R. G. Lim, A. D. Handoko, S. K. Nemani, B. Wyatt, H. Y. Jiang, J. Tang, B. Anasori, Z. W. Seh, ACS Nano 2020; N. Sun, Q. Zhu, B. Anasori, P. Zhang, H. Liu, Y. Gogotsi, B. Xu, Advanced Functional Materials 2019, 29.

[40] Y. Lei, W. Zhao, Y. Zhang, Q. Jiang, J. H. He, A. J. Baeumner, O. S. Wolfbeis, Z. L. Wang, K. N. Salama, H. N. Alshareef, Small 2019, 15, e1901190.

[41] Y. Dong, S. S. K. Mallineni, K. Maleski, H. Behlow, V. N. Mochalin, A. M. Rao, Y. Gogotsi, R. Podila, Nano Energy 2018, 44, 103.
[42] M. Malaki, R. S. Varma, Adv. Mater. 2020, 32, 2003154; G. Song, R. Kang, L. Guo, Z. Ali, X. Chen, Z. Zhang, C. Yan, C.-T. Lin, N. Jiang, J. Yu, New Journal of Chemistry 2020, 44, 7186; L. Guo, Z. Zhang, M. Li, R. Kang, Y. Chen, G. Song, S.-T. Han, C.-T. Lin, N. Jiang, J. Yu, Composites Communications 2020, 19, 134; R. Kang, Z. Zhang, L. Guo, J. Cui, Y. Chen, X. Hou, B. Wang, C. T. Lin, N. Jiang, J. Yu, Sci Rep 2019, 9, 9135.
[43] B. Anasori, Gogotsi, Y. , *2D Metal Carbides and Nitrides (MXenes): Structure, Properties, and Applications*, Springer Nature, Switzerland 2019.
[44] Y. Li, S. Huang, C. Wei, C. Wu, V. N. Mochalin, Nat Commun 2019, 10, 3014.
[45] W. Hong, B. C. Wyatt, S. K. Nemani, B. Anasori, MRS Bulletin 2020, 45, 850.
[46] M. Khazaei, A. Ranjbar, K. Esfarjani, D. Bogdanovski, R. Dronskowski, S. Yunoki, Phys Chem Chem Phys 2018, 20, 8579.
[47] T. Szabó, A. Szeri, I. Dékány, Carbon 2005, 43, 87.
[48] M. Ghidiu, Lukatskaya, M.R., Zhao, M.Q., Gogotsi, Y., Barsoum, M.B., Nature 2014, 516, 78.
[49] W. Hong, Wyatt, B. C., Nemani, S. K., Anasori, B., MRS Bulletin 2020, Submitted.
[50] A. Mockute, J. Lu, E. J. Moon, M. Yan, B. Anasori, S. J. May, M. W. Barsoum, J. Rosen, Materials Research Letters 2014, 3, 16.
[51] A. S. Ingason, M. Dahlqvist, J. Rosen, J Phys Condens Matter 2016, 28, 433003.
[52] M. Alhabeb, K. Maleski, T. S. Mathis, A. Sarycheva, C. B. Hatter, S. Uzun, A. Levitt, Y. Gogotsi, Angew Chem Int Ed Engl 2018, 57, 5444.
[53] Y. Li, H. Shao, Z. Lin, J. Lu, L. Liu, B. Duployer, P. O. A. Persson, P. Eklund, L. Hultman, M. Li, K. Chen, X. H. Zha, S. Du, P. Rozier, Z. Chai, E. Raymundo-Pinero, P. L. Taberna, P. Simon, Q. Huang, Nat Mater 2020, 19, 894.
[54] P. Urbankowski, B. Anasori, T. Makaryan, D. Er, S. Kota, P. L. Walsh, M. Zhao, V. B. Shenoy, M. W. Barsoum, Y. Gogotsi, Nanoscale 2016, 8, 11385.
[55] V. Kamysbayev, Filatov, A.S., Hu, H., Rui, X., Lagunas, F., Wang, D., Klie, R.F., Talapin, D.V., Science 2020.
[56] J. Haglund, A. Fernandez Guillermet, G. Grimvall, M. Korling, Phys Rev B Condens Matter 1993, 48, 11685.
[57] M. Naguib, Mashtalir, O., Carle, J., Presser, V., Lu, J., Hultman, L., Gogotsi, Y., Barsoum, M.W., ACS Nano 2012, 6, 1322.
[58] Q. Tao, M. Dahlqvist, J. Lu, S. Kota, R. Meshkian, J. Halim, J. Palisaitis, L. Hultman, M. W. Barsoum, P. O. Persson, Nature communications 2017, 8, 1.
[59] J. L. Hart, K. Hantanasirisakul, A. C. Lang, B. Anasori, D. Pinto, Y. Pivak, J. T. van Omme, S. J. May, Y. Gogotsi, M. L. Taheri, Nat Commun 2019, 10, 522.
[60] K. Maleski, V. N. Mochalin, Y. Gogotsi, Chemistry of Materials 2017, 29, 1632.
[61] K. Hantanasirisakul, M. Alhabeb, A. Lipatov, K. Maleski, B. Anasori, P. Salles, C. Ieosakulrat, P. Pakawatpanurut, A. Sinitskii, S. J. May, Y. Gogotsi, Chemistry of Materials 2019, 31, 2941.
[62] J. Xuan, Z. Wang, Y. Chen, D. Liang, L. Cheng, X. Yang, Z. Liu, R. Ma, T. Sasaki, F. Geng, Angew Chem Int Ed Engl 2016, 55, 14569; X. Yu, X. Cai, H. Cui, S. W. Lee, X. F. Yu, B. Liu, Nanoscale 2017, 9, 17859.
[63] M. Kurtoglu, M. Naguib, Y. Gogotsi, M. W. Barsoum, MRS Communications 2012, 2, 133.
[64] Z. Guo, J. Zhou, C. Si, Z. Sun, Phys Chem Chem Phys 2015, 17, 15348.
[65] V. N. Borysiuk, V. N. Mochalin, Y. Gogotsi, Nanotechnology 2015, 26, 265705; U. Yorulmaz, A. Ozden, N. K. Perkgoz, F. Ay, C. Sevik, Nanotechnology 2016, 27, 335702; P. Chakraborty, T. Das, D. Nafday, L. Boeri, T. Saha-Dasgupta, Physical Review B 2017, 95.
[66] X.-H. Zha, J. Yin, Y. Zhou, Q. Huang, K. Luo, J. Lang, J. S. Francisco, J. He, S. Du, The Journal of Physical Chemistry C 2016, 120, 15082; Y. Luo, C. Cheng, H. J. Chen, K. Liu, X. L. Zhou, J Phys Condens Matter 2019, 31, 405703; V. N. Borysiuk, V. N. Mochalin, Y. Gogotsi, Computational Materials Science 2018, 143, 418; B. Zhang, W. Zhang, Q. Meng, L. Fan, Q. Zhang, Phys Chem Chem Phys 2019, 21, 1606.
[67] Y.-C. Lu, C.-L. Ren, C.-Y. Wang, Y.-R. Yin, H. Han, W. Zhang, P. Huai, Nuclear Science and Techniques 2019, 30; S. A. Kazemi, Y. Wang, J Phys Condens Matter 2020, 32, 11LT01; W. Jin, S. Wu, Z. Wang, Physica E: Low-dimensional Systems and Nanostructures 2018, 103, 307.
[68] X.-H. Zha, K. Luo, Q. Li, Q. Huang, J. He, X. Wen, S. Du, EPL (Europhysics Letters) 2015, 111; R. Khaledialidusti, B. Anasori, A. Barnoush, Phys Chem Chem Phys 2020, 22, 3414.
[69] L. Feng, X.-H. Zha, K. Luo, Q. Huang, J. He, Y. Liu, W. Deng, S. Du, Journal of Electronic Materials 2017, 46, 2460.
[70] Z. H. Fu, Q. F. Zhang, D. Legut, C. Si, T. C. Germann, T. Lookman, S. Y. Du, J. S. Francisco, R. F. Zhang, Physical Review B 2016, 94.
[71] F. CALDERAZZO, Pure and Applied Chemistry 1960, 33.
[72] M. W. Barsoum, *MAX Phases: Properties of Machinable Ternary Carbides and Nitrides*, Wiley-VCH, 2013.
[73] R. H. Sunil D. Wijeyesekera, American Chemical Society 1984, 3.
[74] J. L. Yongfan Zhang, Lixin Zhou, Shengchang Xiang, Solid State Communications 2002, 121, 411.
[75] M. S. J. A, J. L. BEAUCHAMP, Chem. Rev. 1990, 90, 629.
[76] P. E. M. Siegbahn, J. Phys. Chem. 1995, 99, 12723; G. L. Gutsev, L. Andrews, J. C. W. Bauschlicher, Theoretical Chemistry Accounts: Theory, Computation, and Modeling (Theoretica Chimica Acta) 2003, 109, 298.
[77] K. H. TOKIO YAMABE, TSUTOMU MINATO, KENICHI FUKUI, Inorg Chem 1980, 19, 2154.
[78] S. Huang, V. N. Mochalin, ACS Nano 2020, 14, 10251.
[79] S. H. Jhi, S. G. Louie, M. L. Cohen, J. Ihm, Phys Rev Lett 2001, 86, 3348.

[80] M. W. Barsoum, *Fundamentals of Ceramics*, Vol. 4, Institute of Physics, 2003.
[81] P. Pyykko, M. Atsumi, Chemistry 2009, 15, 186.
[82] C. Kral, W. Lengauer, D. Rafaja, P. Ettmayer, Journal of Alloys and Compounds 1998, 29.
[83] E. Török, Perry, A. J., Chollet, L., & Sproul, W. D. , Thin Solid Films 1987, 153, 37.
[84] Y. Yang, H. Lu, C. Yu, J. M. Chen, Journal of Alloys and Compounds 2009, 485, 542; R. F. Zhang, S. H. Sheng, S. Veprek, Scripta Materialia 2013, 68, 913; E. I. Isaev, S. I. Simak, I. A. Abrikosov, R. Ahuja, Y. K. Vekilov, M. I. Katsnelson, A. I. Lichtenstein, B. Johansson, Journal of Applied Physics 2007, 101.
[85] Z. Fu, D. Legut, T. C. Germann, C. Si, S. Du, J. S. Francisco, R. Zhang, Phys Chem Chem Phys 2018, 20, 14608.
[86] X.-X. Yu, G. B. Thompson, C. R. Weinberger, Journal of the European Ceramic Society 2015, 35, 95.
[87] T. P. Senftle, S. Hong, M. M. Islam, S. B. Kylasa, Y. Zheng, Y. K. Shin, C. Junkermeier, R. Engel-Herbert, M. J. Janik, H. M. Aktulga, T. Verstraelen, A. Grama, A. C. T. van Duin, npj Computational Materials 2016, 2.
[88] V. T. Tom Ziegler, Polyhedron 1987, 6, 685.
[89] K. A. Moltved, K. P. Kepp, The Journal of Physical Chemistry C 2019, 123, 18432; J. C. Sheldon, Australian Journal of Chemistry 1964, 17, 1191.
[90] T. F. Magnera, David, D.E., Michl, J., Journal of the American Chemical Society 1989, 111, 4100.
[91] P. E. M. Siegbahn, Theor. Chim. Acta 1993, 87, 441.
[92] P. E. M. Siegbahn, Chemical Physical Letters 1993, 201.
[93] Y. Sliozberg, J. Andzelm, C. B. Hatter, B. Anasori, Y. Gogotsi, A. Hall, Composites Science and Technology 2020, 108124.
[94] J. Halim, S. Kota, M. R. Lukatskaya, M. Naguib, M.-Q. Zhao, E. J. Moon, J. Pitock, J. Nanda, S. J. May, Y. Gogotsi, M. W. Barsoum, Advanced Functional Materials 2016, 26, 3118.
[95] R. Meshkian, M. Dahlqvist, J. Lu, B. Wickman, J. Halim, J. Thornberg, Q. Tao, S. Li, S. Intikhab, J. Snyder, M. W. Barsoum, M. Yildizhan, J. Palisaitis, L. Hultman, P. O. A. Persson, J. Rosen, Adv Mater 2018, 30, e1706409.
[96] B. Anasori, M. Dahlqvist, J. Halim, E. J. Moon, J. Lu, B. C. Hosler, E. a. N. Caspi, S. J. May, L. Hultman, P. Eklund, J. Rosén, M. W. Barsoum, Journal of Applied Physics 2015, 118; B. Anasori, Y. Xie, M. Beidaghi, J. Lu, B. C. Hosler, L. Hultman, P. R. C. Kent, Y. Gogotsi, M. W. Barsoum, ACS Nano 2015, 9, 9507.
[97] M. Khazaei, A. Ranjbar, M. Arai, S. Yunoki, Physical Review B 2016, 94.
[98] D. Pinto, B. Anasori, H. Avireddy, C. E. Shuck, K. Hantanasirisakul, G. Deysher, J. R. Morante, W. Porzio, H. N. Alshareef, Y. Gogotsi, Journal of Materials Chemistry A 2020, 8, 8957.
[99] G. Deysher, C. E. Shuck, K. Hantanasirisakul, N. C. Frey, A. C. Foucher, K. Maleski, A. Sarycheva, V. B. Shenoy, E. A. Stach, B. Anasori, ACS Nano 2019, 14, 204.
[100] G. Liu, Q. Li, N. Qiu, J. He, Q. Huang, K. Luo, F. Lin, C.-T. Lin, S. Du, Computational and Theoretical Chemistry 2016, 1090, 58.
[101] M. Khazaei, M. Arai, T. Sasaki, M. Estili, Y. Sakka, J Phys Condens Matter 2014, 26, 505503.
[102] R. Meshkian, Q. Tao, M. Dahlqvist, J. Lu, L. Hultman, J. Rosen, Acta Materialia 2017, 125, 476; Q. Tao, M. Dahlqvist, J. Lu, S. Kota, R. Meshkian, J. Halim, J. Palisaitis, L. Hultman, M. W. Barsoum, P. O. A. Persson, J. Rosen, Nat Commun 2017, 8, 14949.
[103] D. Zhang, M. Ashton, A. Ostadhossein, A. C. T. van Duin, R. G. Hennig, S. B. Sinnott, ACS Appl Mater Interfaces 2017, 9, 34467.
[104] H. Zhang, Z. H. Fu, D. Legut, T. C. Germann, R. F. Zhang, RSC Advances 2017, 7, 55912.
[105] T. Hu, M. Hu, Z. Li, H. Zhang, C. Zhang, J. Wang, X. Wang, Phys Chem Chem Phys 2016, 18, 20256.
[106] S. Zhang, T. Ma, A. Erdemir, Q. Li, Materials Today 2019, 26, 67.
[107] J. Yang, B. Chen, H. Song, H. Tang, C. Li, Crystal Research and Technology 2014, 49, 926.
[108] Y. Liu, X. Zhang, S. Dong, Z. Ye, Y. Wei, Journal of Materials Science 2017, 52, 2200.
[109] H. Zhang, T. Hu, X. Wang, Y. Zhou, Journal of Materials Science & Technology 2020, 38.
[110] X. Zhang, M. Xue, X. Yang, Z. Wang, G. Luo, Z. Huang, X. Sui, C. Li, RSC Advances 2015, 5, 2762.
[111] M. Xue, Z. Wang, F. Yuan, X. Zhang, W. Wei, H. Tang, C. Li, RSC Advances 2017, 7, 4312.
[112] X. Zhang, Y. Guo, Y. Li, Y. Liu, S. Dong, Chinese Chemical Letters 2019, 30, 502.
[113] J. Chen, W. Zhao, Tribology International 2021, 153, 106598.
[114] T. Mathis, Maleski, K., Goad, A., Sarycheva, A., Anayee, M., Foucher, A.C., Hantanasirisakul, K., Stach, E., Gogotsi, Y., ChemRxiv 2020.
[115] W. Lian, Y. Mai, C. Liu, L. Zhang, S. Li, X. Jie, Ceramics International 2018, 44, 20154.
[116] A. Rosenkranz, P. G. Grützmacher, R. Espinoza, V. M. Fuenzalida, E. Blanco, N. Escalona, F. J. Gracia, R. Villarroel, L. Guo, R. Kang, F. Mücklich, S. Suarez, Z. Zhang, Applied Surface Science 2019, 494, 13.
[117] M. Marian, G. C. Song, B. Wang, V. M. Fuenzalida, S. Krauß, B. Merle, S. Tremmel, S. Wartzack, J. Yu, A. Rosenkranz, Applied Surface Science 2020, 531.
[118] M. Marian, S. Tremmel, S. Wartzack, G. Song, B. Wang, J. Yu, A. Rosenkranz, Applied Surface Science 2020, 523.
[119] a) Y. Guo, X. Zhou, D. Wang, X. Xu, Q. Xu, Langmuir 2019, 35, 14481; b) Rodriguez, A., Jaman, M. S., Acikgoz, O., Wang, B., Yu, J., Grützmacher, P. G., Rosenkranz, A. & Baykara, M. Z. Applied Surface Science, 525, 147664.
[120] Y. Guan, M. Zhang, J. Qin, X. Ma, C. Li, J. Tang, The Journal of Physical Chemistry C 2020, 124, 13664.
[121] X. Zhou, Y. Guo, D. Wang, Q. Xu, Tribology International 2020, 153, 106646.
[122] H. Zhang, L. Wang, Q. Chen, P. Li, A. Zhou, X. Cao, Q. Hu, Materials & Design 2016, 92, 682.
[123] H. Zhang, L. Wang, A. Zhou, C. Shen, Y. Dai, F. Liu, J. Chen, P. Li, Q. Hu, RSC Advances 2016, 6, 87341.
[124] H. Yan, L. Zhang, H. Li, X. Fan, M. Zhu, Carbon 2020, 157, 217.

[125] F. Meng, Z. Zhang, P. Gao, R. Kang, Y. Boyjoo, J. Yu, T. Liu, Friction 2020.
[126] H. Yan, M. Cai, W. Li, X. Fan, M. Zhu, Journal of Materials Science & Technology 2020, 54, 144.
[127] Y. J. Mai, Y. G. Li, S. L. Li, L. Y. Zhang, C. S. Liu, X. H. Jie, Journal of Alloys and Compounds 2019, 770, 1.
[128] J. Hu, S. Li, J. Zhang, Q. Chang, W. Yu, Y. Zhou, Chinese Chemical Letters 2020, 31, 996.
[129] H. Yan, J. Wang, C. Meng, X. Wang, S. Song, X. Fan, L. Zhang, H. Li, W. Li, M. Zhu, Corrosion Science 2020, 174.
[130] X. Yin, J. Jin, X. Chen, A. Rosenkranz, J. Luo, Advanced Engineering Materials 2020, 22.
[131] A. P. Asia Sarycheva, Yuqiao Liu, Kapil Dandekar, Babak Anasori, Yury Gogotsi, Sci Adv 2018, 4, 1.
[132] M. Anayee, N. Kurra, M. Alhabeb, M. Seredych, M. N. Hedhili, A. H. Emwas, H. N. Alshareef, B. Anasori, Y. Gogotsi, Chem Commun (Camb) 2020, 56, 6090.
[133] V. Natu, R. Pai, M. Sokol, M. Carey, V. Kalra, M. W. Barsoum, Chem 2020, 6, 616; J. Halim, M. R. Lukatskaya, K. M. Cook, J. Lu, C. R. Smith, L. A. Naslund, S. J. May, L. Hultman, Y. Gogotsi, P. Eklund, M. W. Barsoum, Chem Mater 2014, 26, 2374.
[134] M. Seredych, C. E. Shuck, D. Pinto, M. Alhabeb, E. Precetti, G. Deysher, B. Anasori, N. Kurra, Y. Gogotsi, Chemistry of Materials 2019, 31, 3324.
[135] S. Huang, V. N. Mochalin, Inorg Chem 2019, 58, 1958.
[136] V. Natu, J. L. Hart, M. Sokol, H. Chiang, M. L. Taheri, M. W. Barsoum, Angew Chem Int Ed Engl 2019, 58, 12655.